Research Square

Preprints are preliminary reports that have not undergone peer review.
They should not be considered conclusive, used to inform clinical practice,
or referenced by the media as validated information.

Turning Fiber into Earthquake Sensors: Integrated Sensing and Communication in Live FTTH Networks

Emanuele Virgillito

emanuele.virgillito@polito.it

Politecnico di Torino

Federico Notarstefano

Istituto Nazionale di Ricerca Metrologica

Andrè Herrero

Istituto Nazionale di Geofisica e Vulcanologia

Gilda Currenti

Istituto Nazionale di Geofisica e Vulcanologia

Miriana Corsaro

Istituto Nazionale di Geofisica e Vulcanologia

Michele Prestifilippo

Istituto Nazionale di Geofisica e Vulcanologia

Rudi Bratovich

SM-Optics

Raffaele Corsini

SM-Optics

Simone Donadello

Istituto Nazionale di Ricerca Metrologica

Cecilia Clivati

Istituto Nazionale di Ricerca Metrologica

Davide Calonico

Istituto Nazionale di Ricerca Metrologica

Marianna Hovsepyan

Open Fiber

Francesco Carpentieri

Open Fiber

Vittorio Curri

Politecnico di Torino

Article

Keywords:

Posted Date: September 2nd, 2026

DOI: https://doi.org/10.21203/rs.3.rs-10727727/v1

License: This work is licensed under a Creative Commons Attribution 4.0 International License.
Read Full License

Additional Declarations: No competing interests reported.

Turning Fiber into Earthquake Sensors: Integrated Sensing and Communication in Live FTTH Networks

Emanuele Virgillito[1,*], Federico Notarstefano[1,2], André Herrero[3], Gilda Currenti[4], Miriana Corsaro[4], Michele Prestifilippo[4], Rudi Bratovich[6], Raffaele Corsini[6], Simone Donadello[2], Cecilia Clivati[2], Davide Calonico[2], Marianna Hovsepyan[7], Francesco Carpentieri[7], and Vittorio Curri[1]

[1]Politecnico di Torino, Italy
[2]INRIM, Torino, Italy
[3]Osservatorio Nazionale Terremoti, INGV, Roma, Italy
[4]Osservatorio Etneo, INGV, Catania, Italy
[5]Osservatorio Vesuviano, INGV, Napoli, Italy
[6]SM-Optics, Cologno Monzese, Italy
[7]Open Fiber, Roma, Italy
[*]emanuele.virgillito@polito.it

ABSTRACT

Optical telecommunication networks offer a geographically pervasive infrastructure for environmental monitoring alongside data transmission. We investigate earthquake detection through state-of-polarization (SOP) sensing on operational, buried fiber-to-the-home (FTTH) links in Campi Flegrei, a densely populated and highly seismic area. We compare path-integrated SOP measurements obtained with a low-complexity polarization-beam-splitter receiver against reference measurements from coherent interferometry, distributed acoustic sensing, and a conventional seismic station. Four earthquakes recorded in November 2025, with duration magnitudes from 1.9 to 3.3, produced SOP signatures whose timing and spectral evolution were consistent with the available reference measurements and predicted seismic-wave arrivals. During the seismic sequence spanning 31 July and 1 August 2026, which began with a magnitude 4.7 event, manual inspection identified SOP signatures for 10 of the 16 catalogued events with magnitude above 2, including successive events separated by less than one minute. Detection varied between fiber routes because of differences in cable coupling, background noise, and polarization operating point. These results show that low-complexity SOP monitoring can provide complementary seismic observations over live FTTH infrastructure and motivate future networks of synchronized receivers for automated detection and event localization.

Introduction

Optical fiber networks form a geographically extensive infrastructure whose primary function is data transmission, with thousands of kilometers of deployed fiber. At the same time, optical fibers exhibit excellent performance as mechanical stress sensors as pressure variations modify the properties of the propagating light. Because of these properties, the integrated sensing and communications (ISAC) paradigm is gaining momentum, allowing optical fiber networks to evolve from passive data carriers into distributed sensing platforms that combine communication and environmental monitoring within a unified infrastructure[1,2]. In this context, information on environmental conditions can be extracted from network streaming telemetry or from dedicated sensors that coexist with data traffic[3–5]. Data gathered from diverse network elements and sensors across the network can then be processed and correlated to extract information about the surrounding environment. This enables network-integrity monitoring functions that can protect telecommunication and urban infrastructure, as well as early-warning systems for natural hazards such as earthquakes, floods, and landslides[6–10]. Seismic monitoring is a particularly relevant application of this concept. Information obtained from the optical network can support and integrate with conventional seismic instrumentation, providing additional observations along routes and at network locations that are already available for telecommunications. Several fiber optic sensing approaches have been proposed, with the most established being the distributed acoustic sensing (DAS)[11–14]. DAS uses a specialized interrogator leveraging on the coherent detection of the Rayleigh backscattered light to observe strain-rate variations from many consecutive fiber sections, providing a highly sensitive and spatially resolved measurement. However, DAS often requires dedicated dark fibers as it is generally not compatible with live data traffic and large deployment costs. Moreover, its reach is limited to a single fiber span as optical amplifiers block backscattered light. Hence, while providing astonishing sensitivity and spatial resolution, all these aspects limit the

scalability of DAS for large-scale seismic monitoring. In addition, the amount of data produced by such spatially resolved sensing technique should not be overlooked. To overcome these limitations, alternative sensing techniques, compatible with data traffic by design are being recently investigated, particularly those based on the monitoring of optical phase and state of polarization (SOP). Optical phase monitoring can be realized by means of coherent interferometry (CI) and allows detecting seismic events by measuring the phase variations of a reference laser signal accumulated along the fiber path. CI is compatible with data traffic and can be implemented on live networks, but it requires an expensive stable optical phase reference as the intrinsic source laser phase noise intensity must not exceed the weak phase perturbations induced by seismic events. This technique has been demonstrated to detect earthquakes with magnitude lower than 2[15–17]. SOP monitoring is instead based on the measurement of the probe light signal polarization rotations accumulated by the optical field along the fiber path. Mechanical stress, bending, and seismic strain modify the local birefringence of an optical fiber and thereby change the polarization transformation accumulated by the propagating field[5,18,19]. Moreover, SOP sensing does not require an absolute phase reference because it measures the differential phase between two orthogonal polarization components, so optical phase noise common to both components cancels from the polarization observable. SOP sensing can be implemented in several ways. An optical polarimeter can record the evolution of the full Stokes vector set, although the deployment cost of multiple units can become excessive[5]. The digital signal processing (DSP) stage of commercial coherent transceivers already estimates the Stokes vectors to recover the received data symbols, and this information can be exploited to implement SOP sensing with no additional hardware cost[20–22]. However, the DSP stage is usually not accessible in commercial transceivers and the exposed available sampling frequency is usually insufficient for many seismic applications. In this paper we employed a low-tech alternative based on a polarization beam splitter (PBS) and direct photodetection. This PBS-based implementation allows observing only a subset of the polarization space with a sensitivity that depends on the polarization state at the device input. However, it has a lower component count to reduce the cost and complexity of deployment, thus enabling scalability on multiple fiber spans of a typical optical communication system. Moreover, it enables SOP sensing using whatever intensity modulated polarized probe signal, such as optical supervisory channel, typically terminated at each fiber span, by tapping only a small portion of their power[23–27]. SOP monitoring has been successfully employed for seismic monitoring in undersea optical fiber cables, as in this playground traditional seismometers network are difficult to deploy and maintain, while it has been less explored in terrestrial optical fiber networks[20–22,28–30]. Indeed, the main drawback of CI and SOP sensing is that they provide the integrated fiber response along the whole fiber length thus lacking of the spatial resolution of DAS and making the event localization a more complex affair, although source inversion technique for integrated measurements have been proposed[30,31]. The lack of spatial resolution is partially mitigated by an enhanced deployability of sensing devices thanks to their lower cost and complexity, while event localization can be realized with time-delay estimation techniques or by triangulation of multiple sensing devices deployed on different fiber spans, thus emerging from network-wide aggregation of measurements[5,10]. Hence, the application of SOP and CI sensing in terrestrial networks has interest not to completely replace purpose-built seismic networks, but to provide additional observations along routes and at network locations that are already available for telecommunications or to

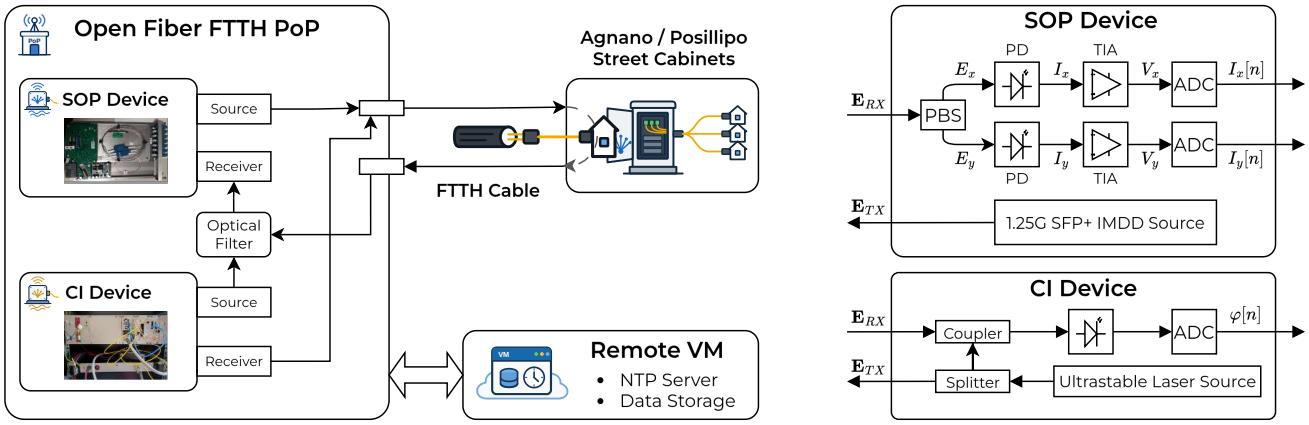


Figure 1. Architecture of the multi-technique sensing testbed. Left: the SOP and CI units installed at the Open Fiber FTTH PoP interrogate looped-back fibers terminating at the Agnano (AGN) and Posillipo (POS) street cabinets; the acquisitions are synchronized through an NTP server and transferred to a remote VM for storage. Upper right: in the simplified SOP receiver, a polarization beam splitter (PBS) separates the received field $\mathbf{E}_{RX}$ into the orthogonal components E_x and E_y, which are photodetected, amplified, and digitized to obtain $I_x[n]$ and $I_y[n]$. Lower right: the CI receiver combines the returned probe with a local reference derived from the source laser and digitizes the interference signal to recover the path-integrated phase $\varphi[n]$.

increase coverage in less populated areas. In this context, the commercial fiber-to-the-home (FTTH) infrastructure is a perfect candidate to implement these techniques. The FTTH network segment combine the geographical pervasiveness and availability of candidate sensing points with shorter fiber spans which can intuitivelylimit the amount of ambient noise accumulated by a path-integrated receiver, thus enhancing the signal-to-noise ratio of the seismic events detection. In this paper we build upon our previous work[5,23,26,32] and demonstrate ISAC paradigm for seismic detection in a live FTTH network owned by the italian telecom operator Open Fiber[33] by exploiting standard data channels without disrupting existing traffic. Our approach leverages SOP fluctuations, captured using a low-complexity PBS-based receiver. In[21] Carver et al. demonstrate earthquake detection is demonstrated in terrestrial fiber cables but using the full Stokes vector information, while Skarvang et al.[28] demonstrated the detection using a PBS-based receiver but using a coiled aerial fiber cable dedicated testbed. In this work we show seamless detection of earthquakes using PBS-based SOP sensing device in a typical, fully buried, commercial FTTH cable in the densely populated and highly seismic area of Campi Flegrei, achieving sensitivity down to magnitude 1.9 events. Particularly, we show the detection of four seismic events happened during November 2025 and a broader seismic sequence spanning 31 July and 1 August 2026 with peak 4.7 magnitude. The SOP earthquake detection is benchmarked against CI technique and independently validated through DAS and co-located conventional seismometers. The results show strong agreement across methods, confirming the reliability of SOP-based sensing for weak seismic signals. These findings establish a scalable and cost-effective paradigm for optical ISAC, transforming existing access networks into pervasive sensing systems. This work paves the way for resilient, dual-use communication infrastructures capable of supporting both high-capacity data transmission and real-time environmental monitoring. In this section we have provided the context of this work. The following section describes the multi-technique sensing testbed and the SOP sensing technique in detail. The subsequent section presents the seismic-event detection and validation results obtained in the live FTTH network. The final section summarizes the conclusions and outlines future perspectives.

Multi-Tech Experimental Testbed in Campi Flegrei

The experimental testbed in the area of Campi Flegrei (Naples, Italy) covers an area of about 7 km wide. Part of it has been established by the Italian operator Open Fiber (OF)[33] as a joint effort with the Italian National Institute of Geophysics and Volcanology (INGV), the Italian National Institute of Metrological Research (INRiM), and the Politecnico di Torino (PoliTo) with the aim to host multiple novel sensing technologies in a highly populated area with a high seismic risk and already equipped with a dense network of conventional seismometers. The testbed is designed to support the development and validation of new sensing techniques for earthquake detection and monitoring, leveraging the existing infrastructure of the FTTH network. The experimental testbed map is reported in Figure 2, while a detailed description of the SOP and CI sensing techniques is depicted in Figure 1. Most seismic activity in Campi Flegrei originates in the so-called *Solfatara di Pozzuoli*, a roughly 700 m-wide area located at the center of the monitored region (and the epicenter of the M3.3 event reported below), although many events also occur throughout the surrounding area, including along the seafront. While SOP and CI sensing operate over the OF FTTH

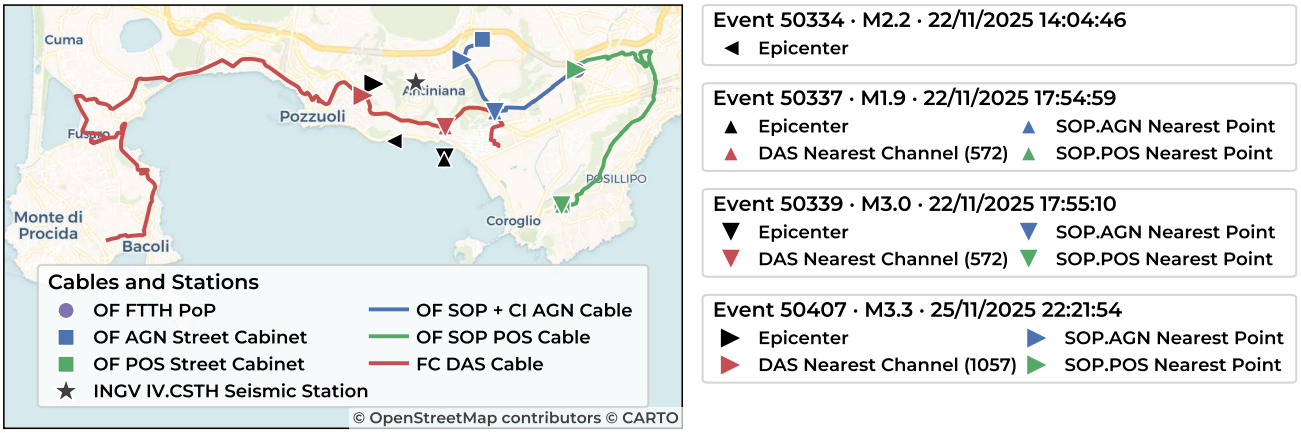


Figure 2. Geographical layout of the Campi Flegrei multi-technique sensing testbed and selected November 2025 earthquakes. The map shows the Open Fiber PoP, the Agnano and Posillipo street cabinets, the CSTH conventional seismic station, the AGN fiber monitored by SOP and CI, the POS fiber monitored by SOP, and the FiberCop cable interrogated by DAS. Event symbols indicate the catalogued epicenters and, where complementary measurements were available, the nearest DAS channel and the nearest points on the two SOP-monitored routes. Event identifiers, magnitudes, and origin times are reported in the legend.

infrastructure, for some events INGV also provided DAS recordings acquired over a dark fiber in a separate FTTH cable owned by the Italian telecommunications operator FiberCop (FC). Other fibers in the same cable carry live traffic; the DAS route is shown in red in Figure 2. DAS data is used here as a complementary reference for the SOP and CI measurements because DAS is an established technique for seismic monitoring. The DAS cable is 22 km long and extends from the FC central office in Bagnoli to the FC central office in Bacoli, traversing the city of Pozzuoli[34]. The DAS interrogator is a Febus A1 operated with a 10 m gauge length. The spatial sampling is 4.8 m, providing 4587 spatial channels. The sampling frequency is limited to 200 Hz to control the data volume while covering the frequency range relevant to the seismic signals considered here. Among the conventional seismic stations deployed in the area, we selected CSTH, which is part of the IV INGV national seismic network, as the reference station (marker in Figure 2).

PBS-based SOP Sensing Configuration

The SOP sensing technique is deployed in a loop-back configuration over two OF FTTH cable segments that depart in opposite directions from the OF FTTH point of presence (PoP) (circle marker in Figure 2). One cable is 4.25 km long and terminates at a street cabinet in Agnano (AGN) (blue cable in Figure 2). The second cable is 7.25 km long and terminates at a street cabinet in Posillipo (POS) (green cable in Figure 2). Both cables cross densely populated areas and are buried underground, thus being subject to anthropogenic noise. The sensing-system configuration is shown in the left panel of Figure 1. The device was designed and produced jointly by the telecommunications vendor SM-Optics and Politecnico di Torino. It is hosted at the OF FTTH PoP together with the signal source. The device is installed in a typical 19-inch rack for telecom equipment as it is derived from an add-drop multiplexer card, thus simplifying installation in telecom buildings. The SOP source is a commercial 1.25 Gbps intensity-modulated direct-detection (IMDD) transceiver in an SFP+ form factor, of the type commonly used for optical supervisory channels in telecommunications networks. Because the IMDD signal is polarized, and the observable depends on the differential phase between orthogonal polarization components, a phase-stabilized optical source is not required. The source output is split and launched into the AGN and POS cables with a transmitted power of -2 dBm in each fiber. The signal propagates along each fiber and is looped back to the OF FTTH PoP at the corresponding street cabinet. During propagation, external mechanical disturbances, including seismic waves, perturb its polarization. Back at the PoP, a small fraction of the returned signal from each fiber is tapped and sent to the SOP monitoring device, while the remaining power can be used by an IMDD data receiver, thereby enabling coexistence with data services. Open Fiber has not experienced any service disruption during the SOP monitoring experiments, confirming that the sensing system is compatible with live traffic. The SOP monitoring device operates with input powers down to -20 dBm. A close-up of the PBS-based SOP receiver is shown in the upper-right panel of Figure 1. The PBS separates the tapped input field $\mathbf{E}_{RX}$ into the orthogonal components E_x and E_y. Each component is detected by a photodiode, producing the photocurrents I_x and I_y, and is then converted to a voltage by a transimpedance amplifier (TIA). A 12-bit analog-to-digital converter (ADC) samples the two voltages at 100 Hz to obtain the time series $I_x[n]$ and $I_y[n]$. Each sample is timestamped and stored in the internal device memory. Absolute timing is provided by synchronizing the device clock to a remote Network Time Protocol (NTP) server hosted on a virtual machine (VM) in the OF network. Acquisitions are organized into 12 h sessions, which are transferred daily to the remote VM for storage. The X and Y components contain both SOP-dependent variations and common-mode intensity fluctuations. We therefore normalize their difference by the total received power, $I_x[n]+I_y[n]$, to suppress common-mode noise and emphasize SOP variations. The SOP observable used throughout this paper is thus given by the following equation:

$$I_d[n] = \frac{I_x[n] - I_y[n]}{I_x[n] + I_y[n]} \tag{1}$$

The metric in Eq. 1 is dimensionless, bounded within $[-1,1]$, and coincides with the normalized Stokes parameter S_1[35] in the receiver device polarization frame. Although this scheme reduces the complexity and cost of SOP monitoring, it observes only one component of the polarization state and therefore does not capture the full Poincaré sphere: variations along S_2 and S_3 are not measured. Consequently, the detection sensitivity depends on the average SOP at the receiver input. When $\mathbf{E}_{RX}$ is nearly aligned with either PBS axis, the orthogonal component approaches zero and the observable approaches an extreme of the $[-1,1]$ range, reducing sensitivity to small variations. However, slow changes in the average SOP, including those induced by daily temperature variations, can move the receiver away from such low-sensitivity operating points.

Coherent Interferometry Sensing Configuration

The CI system is installed at the OF PoP and operates as a complementary phase-sensitive reference for the SOP measurements. The CI device monitors only the 4.25 km AGN cable segment. The optical probe is propagated from the OF FTTH PoP to the Agnano street cabinet and looped back to the PoP through a second fiber in the same cable. The probe is generated by a commercial compact narrow-linewidth laser, whose phase stability enables the weak phase perturbations induced by seismic

strain to be resolved[15,16]. At the receiver, the returned optical field is mixed with a local reference derived from the same source laser. The resulting interference signal is detected by a photodiode and digitized by an ADC, from which the temporal evolution of the optical phase is recovered. External disturbances modify both the length and refractive index of the fiber and therefore the phase accumulated along the round-trip optical path, thus providing a path-integrated observable with not provide spatial resolution. While the CI acquisitions are originally sampled up to 4 kHz, in this paper we will employ data downsampled to 100 Hz, which is sufficient for the seismic analysis considered here. Data is timestamped using the same remote NTP reference employed by the SOP system and is transferred daily to the remote VM for storage.

Seismic event detection in live FTTH networks

In this section we review the seismic events detected by the SOP sensing system during the field trial in Campi Flegrei. The SOP records are compared with the available CI, DAS, and CSTH measurements to validate the seismic origin of the observed transients. The analysis focuses on two periods: a set of four isolated events in November 2025 and a sequence of events spanning 31 July and 1 August 2026. The November 2025 events provide a complete multi-technique comparison, including estimated arrival times of seismic waves P and S phases for SOP, CI and DAS, independently calculated. The July 2026 events are part instead of a seismic sequence started with the M4.7 event on July 31st and followed by several smaller events. For this sequence, only SOP and CSTH data is reported as other techniques were temporarily not available. The earthquake search was based on the event list provided by the INGV - Osservatorio Vesuviano GOSSIP catalog[36]. For each catalogued event occurring during an SOP acquisition session, a time window of about $\pm$30 seconds around each event was inspected manually to determine whether a corresponding transient was visible in either of the two SOP records. This procedure is intended here as an observational assessment of the available data, rather than as an automated event-detection algorithm. The CSTH vertical-component seismogram is reported for every selected event as the principal reference measurement. The CSTH instrument response is removed using the ObsPy tool[37]. CI and DAS records are included when available to provide complementary comparisons with the path-integrated SOP response and the spatially-resolved measurements. All the waveforms have been resampled to 100 Hz and the linear trend has been removed, no further filtering has been applied thus showing all the available content up to 50 Hz. All the spectrogram have been computed on detrended time traces using the Short Time Fourier Transform using a window length of 128 samples (1.28 seconds) and 70% overlap, resulting in a frequency resolution of 0.78 Hz and a time resolution of 0.38 seconds. The time waveform has been normalized to unitary energy prior to the spectrogram computation, in

			Visible Event Signature					Epicentral Distance to Nearest Point (km)		
Event ID	Origin time (UTC)	M_d	SOP	CI	DAS	CSTH	Nearest DAS Channel ID	DAS	SOP.AGN	SOP.POS
November 2025 Events										
50334	2025-11-22 14:04:46	2.2	✓	n.a.	n.a.	✓	n.a.	n.a.	n.a.	n.a.
50337	2025-11-22 17:54:59	1.9	✓	n.a.	✓	✓	572	0.72	1.55	2.82
50339	2025-11-22 17:55:10	3.0	✓	n.a.	✓	✓	572	0.68	1.51	2.82
50407	2025-11-25 22:21:54	3.3	✓	✓	✓	✓	1057	0.35	2.05	4.55
M4.7 31 July 2026 Sequence										
53787	2026-07-31 17:46:43	4.7	✓	n.a.	n.a.	✓	n.a.	n.a.	n.a.	n.a.
53883	2026-07-31 20:00:09	3.8	✓	n.a.	n.a.	✓	n.a.	n.a.	n.a.	n.a.
53925	2026-07-31 21:34:47	2.7	✓	n.a.	n.a.	✓	n.a.	n.a.	n.a.	n.a.
53926	2026-07-31 21:35:39	3.1	✓	n.a.	n.a.	✓	n.a.	n.a.	n.a.	n.a.
54002	2026-07-31 23:20:13	3.1	✓	n.a.	n.a.	✓	n.a.	n.a.	n.a.	n.a.
54017	2026-08-01 00:07:23	2.3	✓	n.a.	n.a.	✓	n.a.	n.a.	n.a.	n.a.
54025	2026-08-01 00:07:31	2.5	✓	n.a.	n.a.	✓	n.a.	n.a.	n.a.	n.a.
54085	2026-08-01 03:47:12	3.1	✓	n.a.	n.a.	✓	n.a.	n.a.	n.a.	n.a.
54088	2026-08-01 03:49:26	3.0	✓	n.a.	n.a.	✓	n.a.	n.a.	n.a.	n.a.
54136	2026-08-01 05:45:19	2.5	✓	n.a.	n.a.	✓	n.a.	n.a.	n.a.	n.a.

Table 1. Earthquakes identified by manual inspection of the SOP acquisitions and availability of complementary measurements. Event identifiers, origin times, and magnitudes M_d are taken from the INGV–OV GOSSIP catalog. A check mark indicates that an event signature is visible in the corresponding record. In the measurement columns, "n.a." denotes that no record from that technique was available for the comparison; in the spatial columns, it denotes a value that has not been calculated. The final four columns report the DAS channel nearest to each epicenter and the epicentral distances to the nearest points on the DAS, SOP AGN, and SOP POS routes.

order to compare events' frequency distribution among different techniques. Then the spectrogram have been clipped down to -90 dB to enhance the visibility of the main spectral content. The large number of events reported in the area illustrates the demanding seismic context of the field trial: between 22 November 2025 and 1 August 2026, the GOSSIP catalog lists 2170 localized events in Campi Flegrei[36]. Among them, 1898 have reported magnitude $M_d < 2$ and 67 have reported $M_d \geq 2$. No evident trace of smaller magnitude events has been identified in the SOP records, at least by the manual inspection performed in this work. Table 1 summarizes the events selected for the comparisons below and the techniques in which a corresponding signature was identified. Each event is identified by its GOSSIP catalog ID. A check mark denotes a visible event signature, whereas "n.a." indicates that the technique was not available due to maintenance or possible temporary outage.

Detection of the November 2025 Events

The November 2025 observations provide the most complete multi-technique comparison in our dataset up to date. The available systems shared a common absolute time reference within the accuracy permitted by the NTP protocol. SOP and CI shared a common time synchronized from the same NTP server, whereas DAS and CSTH were synchronized to different time sources. The epicenter locations of the four selected events relative to the monitored fiber routes and the CSTH station are shown in Figure 2. In particular, while events 50334, 50337 and 50339 occurred in the seafront area, event 50407 occurred in the *Solfatara di Pozzuoli* area, which is the epicenter of most seismic activity in Campi Flegrei. Each subplot in Figure 3 reports the recorded signals' comparison. Detection of events 50337, 50339, and 50407 has been already presented in[32], all the other events in this paper constitute novelty. The first column of shows the time-domain traces, while the second column shows the corresponding time-frequency spectrogram. When DAS data is available, the reported traces are from the DAS channel closest to the epicenter of the event, while the full spatially-resolved DAS record is reported in the second column in place of the spectrogram. In the time-domain traces, the vertical markers indicate the predicted P- and S-wave arrival times at the corresponding measurement locations. For the reference INGV CSTH reference station waveform, the arrival markers are those available in the GOSSIP catalog, while for the other techniques the arrival times were computed independently using the NonLinLoc method[38] with the Campi Flegrei velocity model[39] choosing the nearest point to the event epicenter on the SOP/CI/DAS fibers. The nearest points and arrival times have not yet been calculated for event 50334; the available nearest-point distances and DAS channel identifiers for the other November events are reported in Table 1. A small transient in the AGN SOP record at a time consistent with the CSTH reference for the event 50334is visible in Figure 3(a), while the POS SOP trace does not show a clear signature. Looking at the traces in the frequency domain however reveals more details: a clear spectral decay compatible with the CSTH reference is visible in the AGN SOP trace, while the POS SOP spectrogram shows a weak trace of the earthquake spectral content. This difference is expected for path-integrated polarization measurements because the response depends on the route-dependent coupling of ground motion to the cable and on the instantaneous polarization operating point of each receiver. As mentioned in the previous section, due to urban placement of the SOP cables and the nature of the sensing technique and device, both SOP traces show more intense background noise with respect to CSTH. Both SOP AGN and POS traces show a constant frequency component throughout the whole time windows at around 20 Hz and 30 Hz, respectively. Their nature is yet to be fully understood and deserve deeper investigations. Similar spectral content is also visible during the other events, except in the AGN trace of event 50407. We believe that these components are not related to the earthquakes, as they are present also in the time windows before and after the events while they must be related to some intermittent source of noise throughout the cable or located in the OF FTTH PoP, such as a network device or a power supply. Although the relative amplitude differs between the AGN and POS measurements, both records exhibit an increase in fluctuations around the seismic arrival. Events 50337 ($M_d = 1.9$) and 50339 ($M_d = 3.0$) occurred only approximately 11 s apart and are shown together in Figure3(b). Here, the estimated arrival time at nearest point of the SOP cables to the earthquake epicenter is perfectly compatible with the waveform perturbations caused by the seismic event. In particular, the S wave arrival on the POS cable is slightly delayed with respect to the others, in accordance with the larger nearest impact point distance from the epicenter. Both the events spectral signatures are here strongly visible in the SOP traces, with the larger event producing a more intense and longer-lasting perturbation and the $M_d = 1.9$ event setting the lowest magnitude event seen with this technique to date. Their decay is compatible with the CSTH reference. Interestingly, the 20 Hz constant frequency in the AGN cable show a strong resonance during the seismic events. The CI system was offline during these events, so the comparison is limited to SOP, DAS, and CSTH. Finally, event 50407 ($M_d = 3.3$) (Figure3(c)) provides the only example for which synchronized SOP, CI, DAS, and CSTH data are all available. The earthquake produces a clear response in the SOP AGN branch, whilst still being visible in the POS branch, and the onset and subsequent higher-amplitude motion are temporally consistent with the CI phase, DAS strain-rate, and CSTH displacement records. The longer decay of the SOP AGN cable is consistent with the CSTH reference and the CI trace running on the same cable, although CI shows a much cleaner signal. The agreement among the predicted arrivals and the independently measured transients supports the seismic origin of the SOP perturbation. The waveform amplitudes should not, however, be compared directly across techniques because SOP, accumulated optical phase, local strain rate, and ground displacement are different physical observables and are reported in different units.

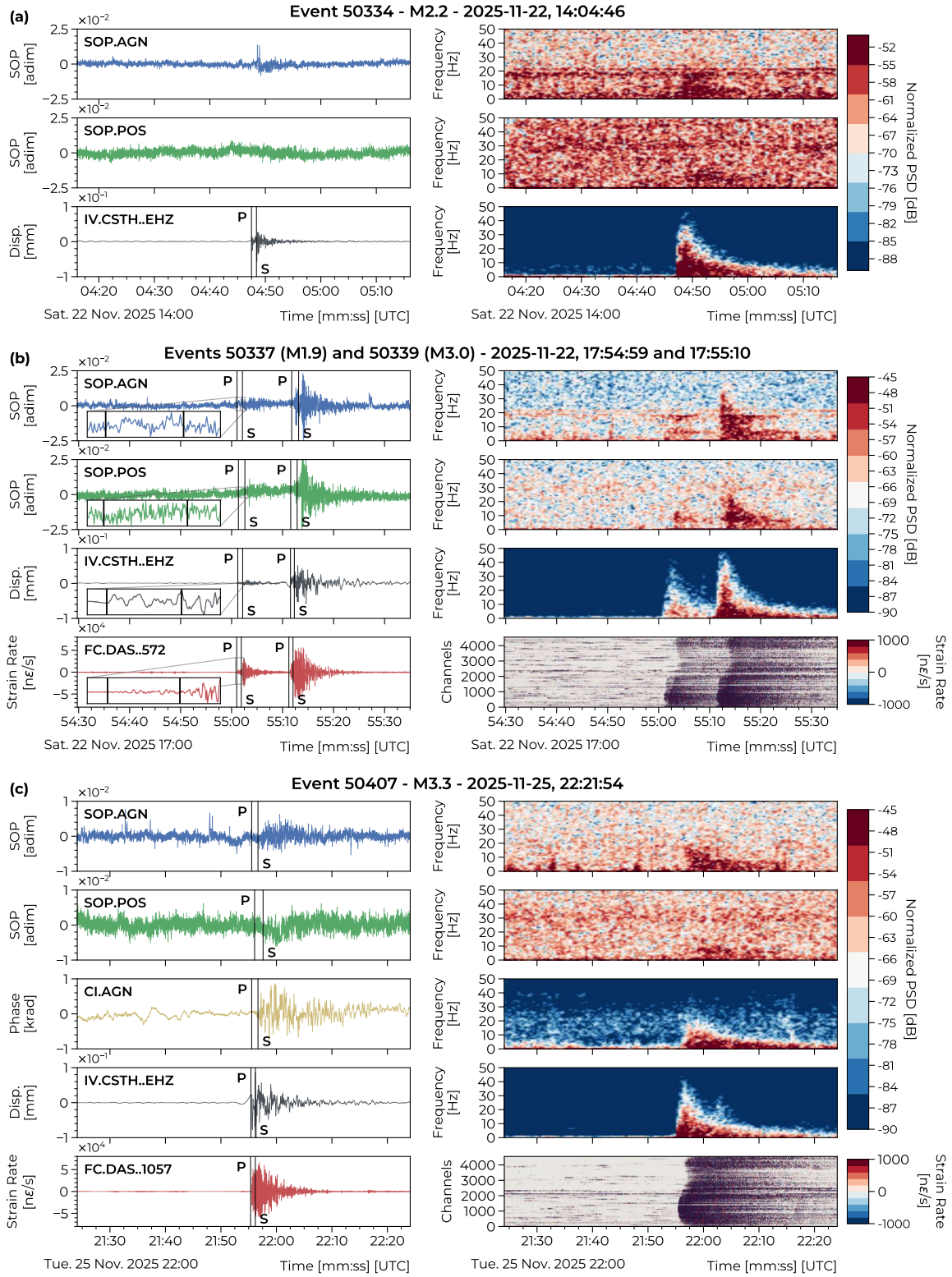


Figure 3. Selected earthquakes recorded in November 2025. The panels show events 50334 ($M_d = 2.2$), 50337 ($M_d = 1.9$) and 50339 ($M_d = 3.0$), and 50407 ($M_d = 3.3$). Time-domain traces are shown on the left and the corresponding time–frequency representations on the right. SOP measurements from the AGN and POS links are compared with the available CI phase, CSTH vertical-component displacement, and DAS strain-rate records. Vertical markers denote the predicted P- and S-wave arrival times.

Detection of the July 2026 Seismic Sequence

Whereas the November measurements mainly concern isolated events or a short two-event pair, the observations in Figure 5 demonstrate the response of the SOP system during an extended seismic sequence compared to the CSTH reference. Figure 4 shows the epicenters of the detected events and their locations relative to the AGN and POS fiber routes. The sequence began with event 53787 at 17:46:43 UTC on 31 July 2026, which had a catalogued magnitude of 4.7, and continued for several hours across midnight. Within the interval from this main event to event 54136 at 05:45:19 UTC on 1 August, GOSSIP reports 16 events with $M_d > 2$[36]. A distinguishable signature was identified manually in the SOP acquisitions for 10 of these 16 events, as listed in Table 1, thus reporting a 62.5% detection rate for this sequence. The remaining six catalogued events did not produce a feature that could be identified confidently above the SOP background in the present manual assessment. During this period, neither CI nor DAS acquisitions were available. A malfunction of the NTP server caused the SOP timestamps to differ from UTC by an unknown, constant offset of around 20 seconds. The absolute SOP timing could therefore not be reconstructed with sufficient accuracy to compare the P- and S-wave arrival times with those recorded at CSTH. Nevertheless, the strength and number of earthquakes occurring within a relatively short interval produced a distinctive succession of transients. A common time shift was consequently determined post-hoc by aligning the complete sequence of SOP features with the CSTH record. This alignment permits association of the SOP transients with individual catalogued events, but it does not constitute an independent validation of absolute SOP timing or seismic-phase arrival times. After applying this common shift, the $M_d = 4.7$ event produces the largest and most persistent SOP response in the sequence and the largest magnitude event verified from the start of the acquisitions, with a clear onset in both the AGN and POS records and an evolution corresponding to the CSTH waveform. Clear SOP transients are also observed for the later $M_d = 3.8$ event 53883 and the $M_d = 3.1$ events 53926, 54002, 54085, and 54088. The two closely spaced pairs, events 53925-53926 and 54017-54025, show that successive earthquakes separated by less than one minute, and in the latter case by approximately 8 s, can leave distinguishable features in the continuously acquired SOP traces. Events 54136 and 54017-54025 are affected by a larger background noise, making their identification less immediate than that of the higher-amplitude events. Looking at the spectral representation, the SOP AGN traces of events 53787 and 53883 seem to show even slight traces of the delayed replicas of the main event clearly visible on CSTH. Overall, events $M_d > 3.0$ show a substantial improvement in their signal-to-noise ratio as the event stands out clearly from the background noise without moving the SOP receiver to a low sensitivity working point. Even lower magnitude events such as 54088 and 54136 which seem to be buried in noise in the time domain in the POS branch are definitely more visible in the frequency domain, showing a clear spectral decay compatible with the CSTH reference. Similarly to the November events, it's interesting to observe the presence of even multiple constant frequency components between 20 Hz and 45 Hz during almost all events. In particular, events 53787 and 53883 show a change of the constant frequency value after a few second from the start of the chose time window. This sudden change may suggest that they are originated by devices fans changing their rotation speed, although this requires further investigation. Overall, the relative responses of the AGN and POS links vary throughout the sequence. Some events are prominent in both traces, whereas others are substantially clearer on one branch. This observation is consistent with the two links sampling different cable routes and with the state-dependent sensitivity of the simplified PBS receiver; it also shows why detection performance cannot be inferred from earthquake magnitude alone. Moreover, the successful detection of this sequence of events started with an event of relatively large intensity constitutes a stress test for the SOP sensing detection capability: while such rapid succession of many powerful events may have altered substantially the average polarization state at the receiver input bringing the SOP device to operate to a low sensitivity working

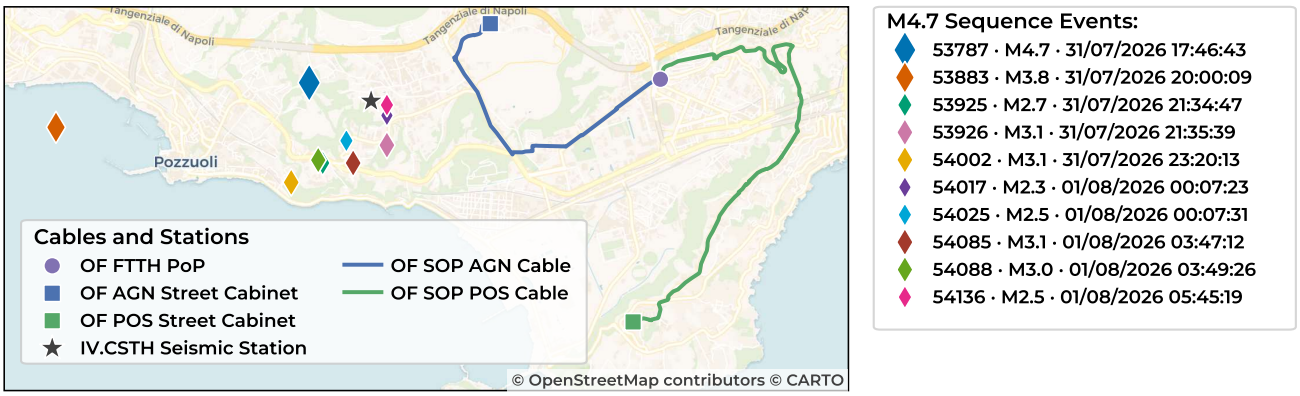


Figure 4. Epicenter locations of the selected events, shown relative to the AGN and POS FTTH fiber routes, the OF PoP, and the two street cabinets. Event identifiers, magnitudes, and catalogued origin times are reported in the legend.

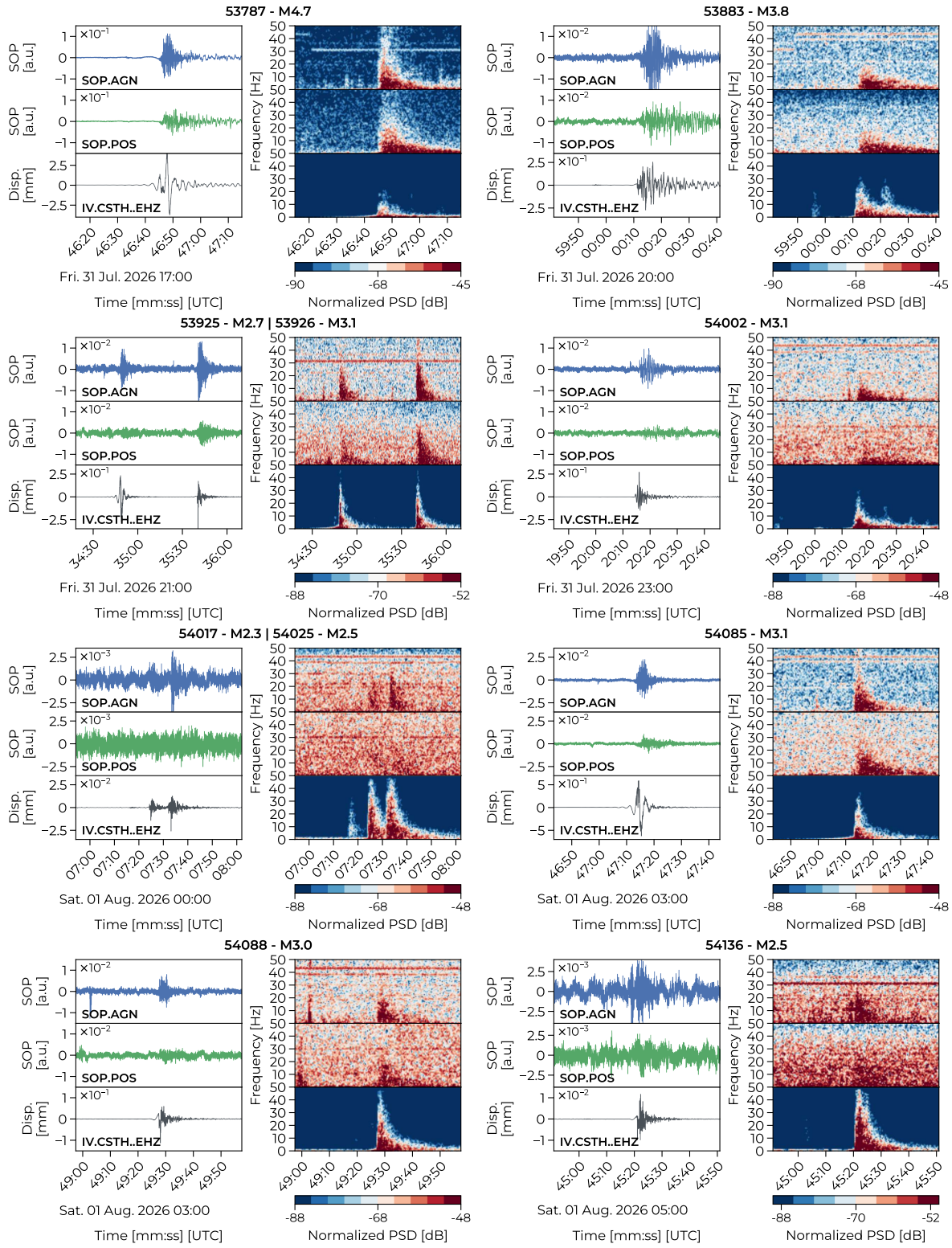


Figure 5. Selected SOP detections. Each panel compares SOP traces acquired on the AGN and POS links with the vertical-component displacement recorded at CSTH. Due to an NTP-server malfunction, the comparison therefore supports event association but not analysis of absolute P- or S-wave arrival times. Event identifiers and magnitudes are reported above each panel; catalogued origin times are listed in Table 1. CI and DAS records were not available for this sequence.

point, the SOP technique has shown robustness and the ability to detect a substantial amount of events.

Conclusions

We deployed a multi-technique fiber-sensing testbed in Campi Flegrei, a densely populated and highly seismic area, to investigate earthquake sensing over operational telecommunication infrastructure. The central contribution is the use of a simplified polarization-beam-splitter receiver to monitor SOP variations on two buried FTTH routes in coexistence with data traffic. CI, DAS and the CSTH seismic station provided complementary measurements with which to evaluate the seismic origin of the SOP perturbations under realistic urban-network conditions and to compare the responses of the different sensing techniques. The principal results are the SOP detection of four November 2025 events, including an event with $M_d = 1.9$, and the observation of the extended sequence spanning 31 July and 1 August 2026. In the November dataset, SOP timing and spectral evolution were consistent with the available CI, DAS, CSTH, and predicted-arrival information. During the M4.7 sequence, SOP signatures were identified by manual inspection for 10 of the 16 catalogued events with $M_d > 2$, including the $M_d = 4.7$ event and pairs separated by less than one minute. The persistence of identifiable SOP signatures throughout this rapid succession of seismic perturbations provides evidence of the robustness of the simplified sensing technique, despite possible changes in the polarization operating point induced by the stronger events. The different responses of the AGN and POS links also show that SOP detectability depends not only on earthquake magnitude, but on cable route, seismic coupling and background noise. These findings show that low-complexity SOP receivers can add seismic-observation capability to live FTTH infrastructure and can complement established seismic instruments and more specialized fiber-sensing systems. The present analysis remains observational: event identification was performed manually, absolute timing was unavailable for the M4.7 sequence, and localization was not demonstrated. Future work will address robust time synchronization, characterization and mitigation of urban noise, automated event detection, and quantitative assessment of sensitivity under different event and link conditions. Deploying multiple accurately synchronized SOP receivers on distinct FTTH routes will also enable investigation of network-level event localization.

References

1. Zhang, Q., Gao, X., Zhang, A., Ding, Y. & Huo, X. Integrated sensing and communication for optical transmission networks. *J. Opt. Commun. Netw.* **18**, B150–B169, DOI: 10.1364/JOCN.584918 (2026).

2. Lu, S. *et al.* Integrated Sensing and Communications: Recent Advances and Ten Open Challenges. *IEEE Internet Things J.* **11**, 19094–19120, DOI: 10.1109/JIOT.2024.3361173 (2024).

3. Sgambelluri, A., Pacini, A., Paolucci, F., Castoldi, P. & Valcarenghi, L. Reliable and scalable Kafka-based framework for optical network telemetry. *J. Opt. Commun. Netw.* **13**, E42–E52, DOI: 10.1364/JOCN.424639 (2021).

4. Ambrosone, R. *et al.* Enabling real-time optical networks as distributed sensors via open-source telemetry architecture. *J. Opt. Commun. Netw.* **18**, B187–B199, DOI: 10.1364/JOCN.587846 (2026).

5. Virgillito, E. *et al.* Multi-tech sensing in-field demonstration on terrestrial optical data networks. *J. Opt. Commun. Netw.* **18**, C37–C48, DOI: 10.1364/JOCN.590101 (2026).

6. Liu, J., Yuan, S., Dong, Y., Biondi, B. & Noh, H. Y. TelecomTM: A Fine-Grained and Ubiquitous Traffic Monitoring System Using Pre-Existing Telecommunication Fiber-Optic Cables as Sensors. *Proc. ACM Interact. Mob. Wearable Ubiquitous Technol.* **7**, 64:1–64:24, DOI: 10.1145/3596262 (2023).

7. Malik, G. *et al.* Resilient Anomaly Detection in Fiber-Optic Networks: A Machine Learning Framework for Multi-Threat Identification Using State-of-Polarization Monitoring. *AI* **6**, DOI: 10.3390/ai6070131 (2025).

8. Landrø, M. *et al.* Sensing whales, storms, ships and earthquakes using an Arctic fibre optic cable. *Sci. Reports* **12**, 19226, DOI: 10.1038/s41598-022-23606-x (2022).

9. Pellegrini, S., Rizzelli, G., Barla, M. & Gaudino, R. Algorithm Optimization for Rockfalls Alarm System Based on Fiber Polarization Sensing. *IEEE Photonics J.* **15**, 1–9, DOI: 10.1109/JPHOT.2023.3281670 (2023).

10. Clivati, C. *et al.* Seismic monitoring and cable supervision on optical data networks: Requirements, challenges, and results. *J. Opt. Commun. Netw.* **18**, C127–C136, DOI: 10.1364/JOCN.590258 (2026).

11. Ajo-Franklin, J. B. *et al.* Distributed acoustic sensing using dark fiber for near-surface characterization and broadband seismic event detection. *Sci. Reports* **9**, 1328, DOI: 10.1038/s41598-018-36675-8 (2019).

12. Lindsey, N. J. & Martin, E. R. Fiber-Optic Seismology. *Annu. Rev. Earth Planet. Sci.* **49**, 309–336, DOI: 10.1146/annurev-earth-072420-065213 (2021).

13. Sladen, A. *et al.* Distributed sensing of earthquakes and ocean-solid Earth interactions on seafloor telecom cables. *Nat. communications* **10**, 1–8 (2019).

14. Jousset, P., Mortensen, A. K., Fridleifsson, G. Ó., Ágústsson, K. & Gudmundsson, M. T. Reykjanes, Iceland: Structure and dynamics of mid-oceanic ridge geo/hydrothermal systems. *J. Volcanol. Geotherm. Res.* **391**, 106692, DOI: 10.1016/j.jvolgeores.2019.106692 (2020).

15. Marra, G. *et al.* Ultrastable laser interferometry for earthquake detection with terrestrial and submarine cables. *Science* **361**, 486–490, DOI: 10.1126/science.aat4458 (2018).

16. Donadello, S., Clivati, C., Govoni, A. *et al.* Seismic monitoring using the telecom fiber network. *Commun. Earth & Environ.* **5**, 1–9, DOI: 10.1038/s43247-024-01338-2 (2024).

17. Bogris, A. *et al.* Sensitive seismic sensors based on microwave frequency fiber interferometry in commercially deployed cables. *Sci. Reports* **12**, 14000, DOI: 10.1038/s41598-022-18130-x (2022).

18. Zhan, Z. *et al.* Optical polarization-based seismic and water wave sensing on transoceanic cables. *Science* **371**, 931–936, DOI: 10.1126/science.abe6648 (2021).

19. Pellegrini, S. *et al.* Overview on the state of polarization sensing: Application scenarios and anomaly detection algorithms. *J. Opt. Commun. Netw.* **17**, A196–A209, DOI: 10.1364/JOCN.537881 (2025).

20. Mecozzi, A. *et al.* Geophysical sensing using Jones matrices extracted from submarine optical cable transceivers carrying live traffic. *Optica* **12**, 1712–1719, DOI: 10.1364/OPTICA.572883 (2025).

21. Carver, C. J. & Zhou, X. Polarization sensing of network health and seismic activity over a live terrestrial fiber-optic cable. *Commun. Eng.* **3**, 1–12, DOI: 10.1038/s44172-024-00237-w (2024).

22. Costa, L., Varughese, S., Mertz, P., Kamalov, V. & Zhan, Z. Localization of seismic waves with submarine fiber optics using polarization-only measurements. *Commun. Eng.* **2**, 1–7, DOI: 10.1038/s44172-023-00138-4 (2023).

23. Straullu, S. *et al.* Real-time detection of anthropic events by 10G channels in metro network segments. In *2022 IEEE Photonics Conference (IPC)*, 1–2, DOI: 10.1109/IPC53466.2022.9975561 (2022).

24. Bjørnstad, S., Ali, J., Dreibholz, T. & Sæthre, E. A scalable data collection system for continuous state of polarisation monitoring. In *2023 23rd International Conference on Transparent Optical Networks (ICTON)*, 1–4, DOI: 10.1109/ICTON59386.2023.10207183 (2023).

25. Yang, B. *et al.* Accurate vibration recognition enabled by synergistic sensing based on both phase and SOP for stable IM-DD optical interconnects. *J. Opt. Commun. Netw.* **18**, B85–B96, DOI: 10.1364/JOCN.584770 (2026).

26. Bratovich, R. *et al.* Surveillance of Metropolitan Anthropic Activities by WDM 10G Optical Data Channels. In *European Conference on Optical Communication (ECOC) 2022 (2022), Paper Tu3B.6*, Tu3B.6 (Optica Publishing Group, 2022).

27. Virgillito, E. *et al.* Detection, Localization and Emulation of Environmental Activities Using SOP Monitoring of IMDD Optical Data Channels. In *2023 23rd International Conference on Transparent Optical Networks (ICTON)*, 1–4, DOI: 10.1109/ICTON59386.2023.10207513 (2023).

28. Vaskinn, K. S. *et al.* Sensing earthquakes in aerial single- and multi-core fiber optic networks. *J. Opt. Commun. Netw.* **18**, B119–B128, DOI: 10.1364/JOCN.584845 (2026).

29. Mecozzi, A. *et al.* Observation of Precursor of the Kamchatka Earthquake by Monitoring an Optical Fiber Link in the Mediterranean Sea, DOI: 10.1364/opticaopen.30273163.v2 (2025).

30. Li, T. *et al.* Submarine integrated sensing and communication cable networks enable high-precision earthquake location estimation through linear wavefront theory. *J. Opt. Commun. Netw.* **18**, B108–B118, DOI: 10.1364/JOCN.585552 (2026).

31. Fichtner, A. *et al.* Theory of phase transmission fibre-optic deformation sensing. *Geophys. J. Int.* **231**, 1031–1039, DOI: 10.1093/gji/ggac237 (2022).

32. Virgillito, E. *et al.* Low-tech SOP sensing over FTTH for seismic monitoring in campi flegrei: Benchmarking against interferometry and ϕ-OTDR (accepted). In *Proceedings of the 2026 European Conference on Optical Communication (ECOC)*, Mo4P.89 (Málaga, Spain, 2026).

33. Open Fiber. Open Fiber. https://openfiber.it/ (2026). Accessed 15 August 2026.

34. Currenti, G. *et al.* Installazione di dispositivi das per il potenziamento del monitoraggio dei campi flegrei. *Rapp. Tec. INGV* DOI: 10.13127/rpt/489 (2025).

35. Collett, E. *Field Guide to Polarization* (SPIE Press, Bellingham, Washington, 2005).

36. Ricciolino, P., Lo Bascio, D. & Esposito, R. GOSSIP - Database Sismologico Pubblico INGV-Osservatorio Vesuviano, DOI: 10.13127/GOSSIP (2024).

37. Krischer, L. *et al.* ObsPy: A bridge for seismology into the scientific Python ecosystem. *Comput. Sci. & Discov.* **8**, 014003, DOI: 10.1088/1749-4699/8/1/014003 (2015).

38. Lomax, A., Virieux, J., Volant, P. & Berge-Thierry, C. Probabilistic earthquake location in 3d and layered models. In Thurber, C. H. & Rabinowitz, N. (eds.) *Advances in Seismic Event Location*, 101–134, DOI: 10.1007/978-94-015-9536-0_5 (Springer Netherlands, Dordrecht, 2000).

39. Tramelli, A., Giudicepietro, F., Ricciolino, P. & Chiodini, G. The seismicity of campi flegrei in the context of an evolving long-term unrest. *Sci. Reports* **12**, DOI: 10.1038/s41598-022-06928-8 (2022).

Acknowledgements

We are grateful to FiberCop staff for granting access to the power station and providing the dark fiber used for DAS measurements.

Funding

Politecnico di Torino, SM-Optics, INGV: This work has been supported by the Open Fiber *Fiber as a Sensing* (FaaS) project. INRiM, INGV: This work has been supported by the Open Fiber MEGLIO project. Politecnico di Torino, Open Fiber, INRiM, INGV, SM-Optics: This work has been supported by the European Union under the SENSEI project (Grant Agreement: 101189545).

Author Contributions

EV: conception and design of the experiment, data collection, post-processing, analysis and manuscript production. FN: contribution to code development, figures and manuscript production. AH: conception and design of the experiment, analysis of the seismic data and interpretation of the SOP data. RB, RF: development and production of the PBS-based SOP device in SM-Optics and its acquisition firmware. GC, MC, MP: DAS data acquisition, processing and evaluation of the NonLinLoc arrival time estimations. SD, CC, DC: development and operation of the CI system and CI data post-processing. MH, FC: coordination of the Open Fiber FaaS project and support for the deployment of the SOP system in the FTTH network. VC: principal investigator, scientific steering, conception and design of the experiment. All authors critically reviewed and approved the manuscript.

Data Availability

Presented data is available from the corresponding author upon reasonable request.

Competing interests

The authors declare no competing interests